Adaptive Threshold Selection of Anisotropic Diffusion Filters Using Dissimilarity Transform

Mahmut Kılıçaslan[1*] iD

[1]Ankara Üniversitesi Nallıhan Vocational School, 06920, Ankara, TÜRKİYE

Abstract
The development of technology has increased the use of imaging devices. In addition, the development of hardware in recent years has improved the quality of images. However, noise in images is inevitable due to many factors during or after the image acquisition process. Image filters are used to remove these noises and this process is an important research area. One of the most basic steps of image processing is denoising. Diffusion filters have been used for denoising for many years, as they protect the edges. The common problem of diffusion filters, which are still being developed today, is the user intervention requirements. The diffusion threshold value is currently selected by the user. In this study, a fully adaptive threshold value selection method is presented with the help of dissimilarity transform. The main contribution of the study is the proposal of dissimilarity transformation for anisotropic diffusion filters. Experimental results show that the threshold values determined by the proposed method effectively provide denoising without being affected by noise variance and preserve the edges.

Key Words
"Anistropic diffusion filter, Adaptive threshold selection, Dissimilarity Transform, Denoising"

*Sorumlu Yazar: m.kilicaslan@ankara.edu.tr

1. Introduction

Image denoising algorithms have used in various different fields such as medicine, defense industry, education or space science. In addition, many identifications, analysis and extraction operations are performed through digital images. Digital images are often corrupted due to the structure of the imaging devices or storage and transfer processes. The elimination of these distortions, called noise, is of great importance for the success of various processes such as segmentation, edge detection, or image retrieval(İncetaş et al., 2017). Therefore, denoising of the images is one of the crucial steps for digital image processing (Gao et al., 2017). The goal of the denoising is to eliminate the noise pixels in the image while preserving the features such as edges (Jain & Tyagi, 2016).

Many noise filters in different structures have been developed to remove noise (Incelas et al., 2014). The anisotropic diffusion filter (ADF), first proposed by Perona and Malik (PM) in 1990 (Perona & Malik, 1990), has been used in many studies on noise reduction. Except for spatial filters that cause distortion of edge pixels, partial differential equation (PDE) based anisotropic diffusion filters can preserve the edges while removing noisy pixels (Yu et al., 2010). The success of the diffusion filter attracted so much attention that new filter models with different diffusion functions were developed in the followed years (Charbonnier et al., 1994; Weickert, 1998). Although these models have different diffusion functions, they are structurally based on PM ADF. In (Ham et al., 2012), a new filter design based on second order PDE has been developed for a more powerful ADF. Subsequently, ADFs based on fourth order PDE were proposed to reduce the staircase effect of second order diffusion filters (Barbu, 2016; Hajiaboli, 2009; You & Kaveh, 2000). In addition to denoising achievement of these techniques, it was stated that they reduce the staircase effect and preserve the edges. In 2019, a fourth-order AD filter, which has a very high edge preservation success, was presented this time as Hessian Matrix-based (Deng et al., 2019). In the evaluations made in terms of both visual and measurement metrics, it has been stated that it provides a better performance than both PM and other fourth order AD filters.

Although different types of filters have been developed, it is often not possible to know the noise intensity. Choosing the most suitable parameters require trial and error and certain expertise, which prolongs the denoising process and increases the cost. For this purpose, adaptive filtering techniques have been developed to reduce the noise effect. Rafsanjani et al. (2016) stated that the diffusion coefficient is of great importance in the success of adaptive filtering (Rafsanjani et al., 2017). They presented a diffusion coefficient calculation approach based on residual local power and the amount of the gradient magnitude. In order to determine the diffusion coefficient adaptively, an approach based on local minimum mean square error (LMMSE) has also been proposed (Aja-Fernández & Alberola-López, 2006). In 2016, a semi-adaptive K threshold selection approach was proposed (Xu et al., 2016). Despite the success of the developed filters, the K threshold value, which is a very important parameter, needs to be determined by the user in the calculation of the diffusion coefficient. It is known that more successful results can be obtained by selecting different K values according to the noise intensity of the image (Rafsanjani et al., 2016).

In recent years, it has been observed that studies on the automatic determination of the K value according to the characteristics of the image have come to the fore. The idea of calculating the K-value using the center of gravity of the wavelet histogram was presented by Demirci and Tanyeri in 2012 (Demirci & Tanyeri, 2012). Then, in 2018, the same authors presented another study developed by Tanyeri and Demirci (TD), in which the K threshold was automatically obtained using the wavelet transform (Tanyeri & Demirci, 2018). They used the average of three values obtained using MAD as the K value for horizontal, vertical, and diagonal wavelet coefficients, and they also indicated that the success rates for speckle images were quite high

In this study, a new approach is presented where the threshold value of the anisotropic diffusion filter is calculated adaptively using dissimilarity transform. First, the dissimilarity transform of the image and the calculation of the corresponding Average Dissimilarity Value (ADS) are introduced. ADS is used to find the K threshold value with the help of an exponential function. Next, the proposed approach is tested on astronomical images using different diffusion functions. The proposed model is compared with both the fixed K values that give the best results and the wavelet-based adaptive technique. Results are made both with known measurement metrics and visually. Laplacian of Gaussian (LoG) edge detection approach, which has a very high noise sensitivity, is also used in the visual evaluation.

2. Theory and Method

2.1. Anisotropic Diffusion Filter and Threshold Value

The nonlinear anisotropic diffusion filter, widely used for denoising while preserving edges, was first proposed by the Perona and Malik (PM) in 1990 (Perona & Malik, 1990). The equation of the filter based on heat diffusion was as follows:

$$\frac{dI(x,y,t)}{dt} = div(c(x,y,t)\,\nabla I(x,y,t)) \tag{1}$$

where div, ∇, and t denote divergence, gradient operator, and time, respectively. In addition, c is called the diffusion or conductivity coefficient and can also be expressed as a function. PM diffusion function is given in Eq. (2). As a result of the equation, the diffusion function value must be between 0 and 1. It is expected that this value will approach to 1 when the noise is high intense and to zero when the noise is low intense, in order to perform the diffusion process correctly.

$$c(x,y,t) = \frac{1}{1 + \left(\|\nabla I\| / K \right)^2} \tag{2}$$

where K is diffusion threshold and given as a constant. To reduce the staircase effect of the PM approach, a new model was proposed using fourth order PDE in the diffusion function (You & Kaveh, 2000)

$$\frac{dI}{dt} = -\nabla^2 \left(c\left(|\nabla^2 I| \right) \nabla^2 I \right) \tag{3}$$

where $\nabla^2 I$ is the image Laplacian and calculated as in Eq. (4).

$$\left| \nabla^2 I \right| = \left| I_{xx} + I_{yy} \right| \tag{4}$$

where I_{xx} and I_{yy} are second order derivatives of I. In (Hajiaboli, 2009), the function in Eq. (5) was proposed by using the Euclidean norm in order to increase the edge preservation feature of the filter.

$$\frac{dI}{dt} = -\nabla^2 \left(c\left(\|\nabla^2 I\| \right) \nabla^2 I \right) \tag{5}$$

Recently, one of the most successful techniques is the Hessian Matrix based fourth order anisotropic diffusion filter (Deng et al., 2019) and the diffusion function has been modified as in Eq. (6).

$$\frac{dI}{dt} = -\nabla^2 \left(c_1 \lambda_1 + c_2 \lambda_2 \right) \tag{6}$$

where λ_1 and λ_2 are the eigenvalues of Hessian Matrix, while c_1 and c_2 are diffusion coefficients and are calculated as in Eq. (7) and Eq. (8).

$$c_1 = c_2{}^2 \tag{7}$$

$$c_2 = \frac{1}{1 + \dfrac{|\lambda_1 - \lambda_2|^2}{K^2}} \tag{8}$$

Although different diffusion functions have been developed for ADFs as mentioned above, the general structure of the filters is as shown in Fig. 1. f (x, y), g (x, y), and K denote the noisy image, the filtered image, and the threshold value.
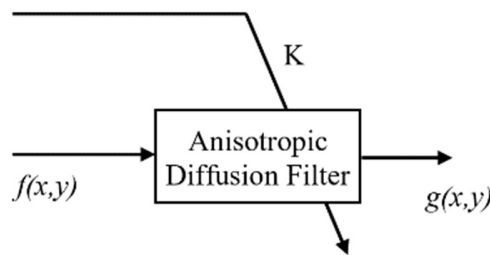

Figure 1. Conventional Diffusion Filter Diagram.

Common disadvantage of the mentioned filters is that the K value is user-defined, although it has a great effect on the success of the ADF (Tsiotsios & Petrou, 2013). Due to the structure of the diffusion equations, it is clear that as the K value increases, diffusion will increase. It is also known that choosing a higher K value in high noisy images and lower K value in low noisy images produces more successful results (Demirci & Tanyeri, 2012).

The most effective approach developed in recent years to determine the K value without user intervention was proposed by Tanyeri and Demirci in 2018 (Tanyeri & Demirci, 2018). First of all, 3 different values were obtained by using the median absolute deviation

process on the horizontal, vertical and diagonal wavelet coefficients of the noisy image. Then the average of these three values was used as the K threshold value.

2.2. Dissimilarity Transform

The idea of using the similarity of pixels instead of Euclidean distance for the purpose of edge detection was first proposed by Demirci (Demirci, 2007) in 2007. Thus, it was possible to detect the edges without making complex calculations. Thanks to its advantages, similarity transform has been used in many studies on segmentation (Guvenc et al., 2008; Incetas et al., 2014; İncetaş & Uçar, 2021; M. O. İncetaş et al., 2017) and edge detection (Ali, 2013; Aydın et al., 2016). The similarity transform (SP) of a center pixel (P_0) in a 3x3 neighborhood is calculated using the gray level values of the neighboring pixels as follows:

$$S(P_0, P_i) = \exp\left(-\frac{|P_0 - P_i|}{D_n}\right) \tag{9}$$

$$S_P = \frac{1}{9}\sum_{i=0}^{8} S(P_0, P_i) \tag{10}$$

where $|P_0 - P_i|$ is the absolute difference of gray level values of neighboring pixels and D_n is the user selected normalization coefficient. Therefore, the success of the similarity transformation depends on the coefficient that the user chooses. In 2019, a new approach was introduced that automatically calculates the D_n coefficient used in the similarity transform (INCETAS et al., 2019).

$$D_n = \left(\frac{255}{d_a^2 + 1}\right) + 1 \tag{11}$$

where d_a is the mean of the absolute difference between the P_0 and the other neighbor pixels in the 3x3 mask. It is calculated as:

$$d_a = \frac{1}{9}\sum_{i=0}^{8} d_{0,i} \qquad (i=0, 1, ..., 8) \tag{12}$$

where $d(0,i) = |P_0 - P_i|$ is the absolute difference between P_0 and neighbor pixel, P_i. By this way, the similarity transform is calculated for each pixel locally and automatically, without user dependency.

In this study, the invert of the similarity value, that is, the dissimilarity (DS) value of the pixels was calculated as given below. All gray level values obtained from the DS transform are in the range of [0,1].

$$DS_P = 1 - S_P \tag{13}$$

The noise-free astronomical images used in the study and their DS transforms are shown in Fig. 2. In the DS transform images, it is seen that the gray level values of the pixels in the edge regions close to 1 (white). On the other hand, the DS values approach 0 (black) in regions where the pixels are homogeneous. Although the edge regions become clear as a result of the transform, the similarities between the neighboring pixels in an image are also revealed. The brighter DS transform result means that the image consists of dissimilar pixels. The DS values of the pixels are used in this study to calculate the K threshold value of the anisotropic diffusion filter.
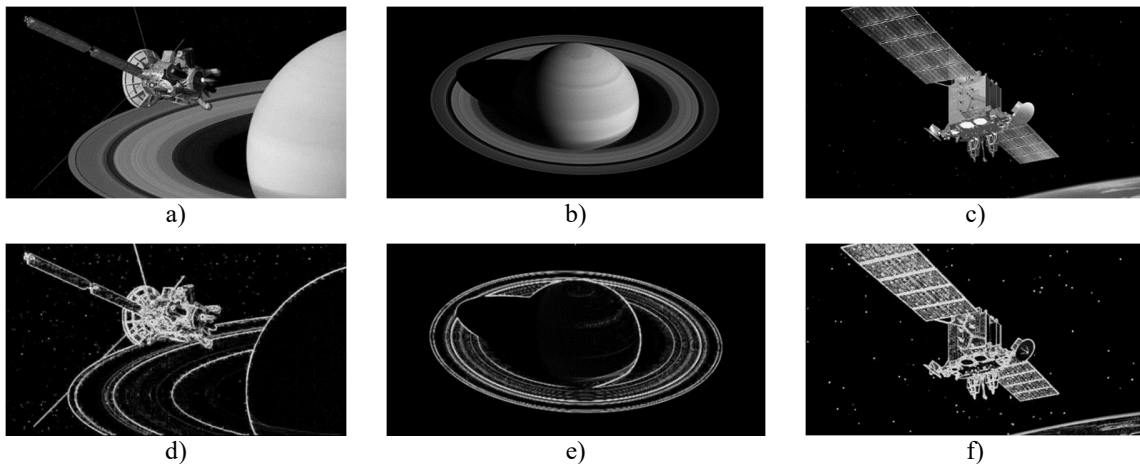

Figure 2. Original images **(a-c)** and dissimilarity transform results **(d-f)**.

2.3. Proposed Adaptive Threshold Selection Model

Although many ADF models successfully remove noise and preserve edges, they need users or complex calculations such as wavelet transforms. In this paper, a simple calculation method using the DS value is proposed instead of manually selecting the threshold value K. The average gray level value (ADS) of the image obtained from the DS transform is calculated.

$$ADS = \frac{1}{M\,N}\sum_{i=0}^{M-1}\sum_{j=0}^{N-1}\Big(DS(x_i, y_j)\Big) \tag{14}$$

where M and N are the width and height values of the image, DS(x, y) is the dissimilarity image, and the ADS is the average dissimilarity value. Thus, important information about the dissimilarity of the pixels in the image is achieved. In the tests, it has been observed that the diffusion filter gives more successful results when there is an exponential relationship between the increase in values of ADS and K. For this purpose, an exponential function in Eq. (15) is used to calculate the K value by means of ADS.

$$K = 255 \cdot ADS \cdot (10^{2\cdot(ADS-1)}) \tag{15}$$

The exponential relationship between the ADS and the K threshold value is shown in Fig. 3. For the K threshold value to be maximum, 255, the ADS value must be 1. To reach the threshold value of K = 50, which is used in many studies, the ADS value greater than 0.70 is required.
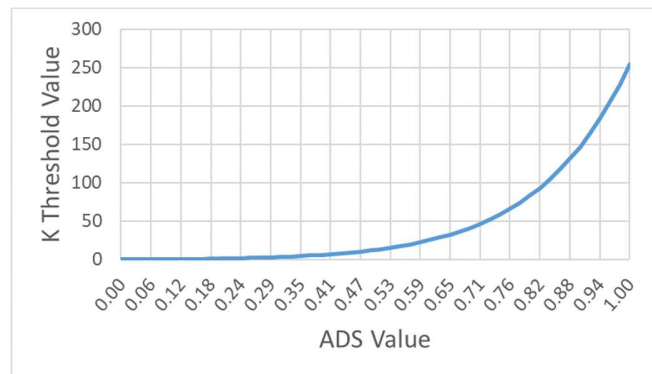

Figure 3. The relationship between ADS and K coefficient.

The change in ADS and K values according to the increase in noise variance for each image is shown in Fig. 4. Especially at the high noise levels, although the difference between ADS values of images is small, the difference between K values increases due to the structure of Eq. (15).
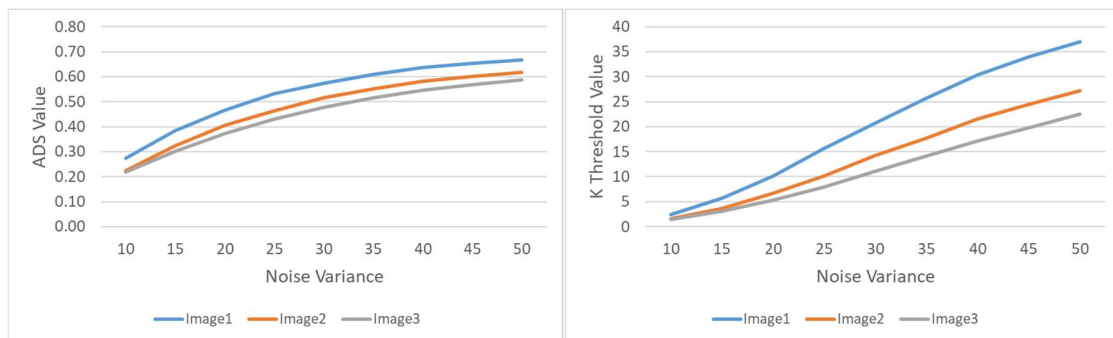

Figure 4. Effect of noise variance on ADS and K coefficient.

The diagram of the proposed method is given in Fig. 5. As can be seen, the K value can be calculated quickly and automatically with a simple mathematical operation using the noisy image, and the user does not need to enter a value anymore.
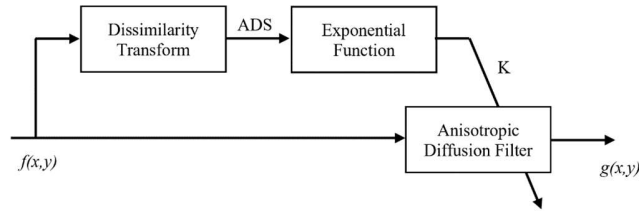
Figure 5. Proposed Diffusion Filter Diagram.

3. Experimental Results

In order to measure the performance of diffusion filters, peak signal to noise ratio (PSNR), and the structural similarity index (SSIM) metrics (Wang et al., 2004), which are considered as important criteria for the similarity of two images, are used. Both PSNR and SSIM metrics determine image quality, and their higher values indicate the higher the success of the filter.

While obtaining the results, 9 different levels of Gaussian noise (σ^2 = 10, 15, 20, 25, 30, 35, 40, 45, 50) are added to the images. In order to test the success of the proposed automatic diffusion threshold selection approach, fourth-order ADFs such as YK(You & Kaveh, 2000) and HM (Deng et al., 2019) are also applied to the noisy images besides the conventional PM ADF. While applying diffusion filters, in addition to the constant K values (K = 10, 25, 50, 75, and 100), the wavelet-based K values (Demirci et al., 2012) and the values calculated with the proposed method in this study are used. PSNR and SSIM values are calculated for the images obtained as a result of the 30th iteration. In Fig. 6(a) and Fig. 7(a), there are three images with gauss σ^2 = 20 and σ^2 = 40 noise, respectively. DS transform results of these noisy images are shown in Fig. 6(b) and Fig. 7(b). As can be seen in the figures, when the noise increases, the DS transforms are brighter, that is, the ADS value is higher.
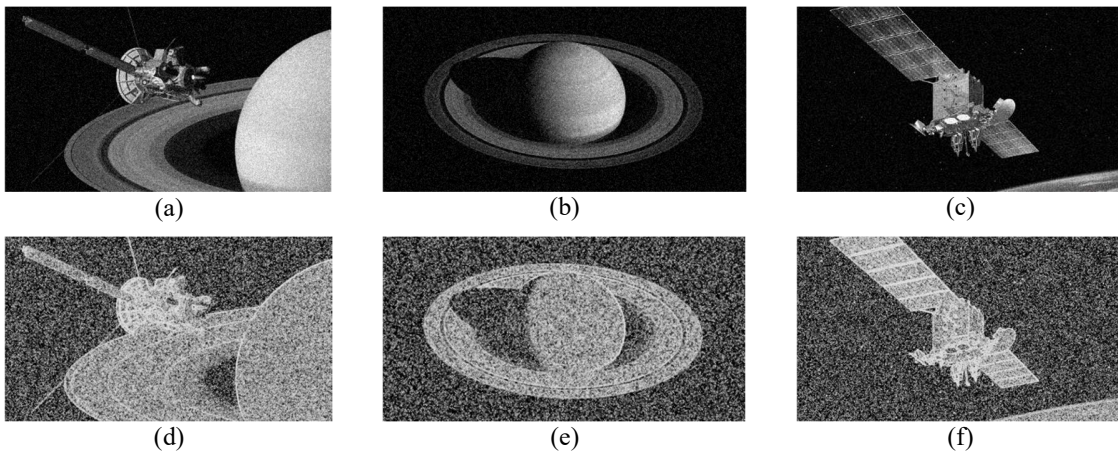

Figure 6. Noisy images and DS Transform results. **(a-c)** Noisy images ($\sigma2$=20), **(d-f)** Results of Dissimilarity Transform
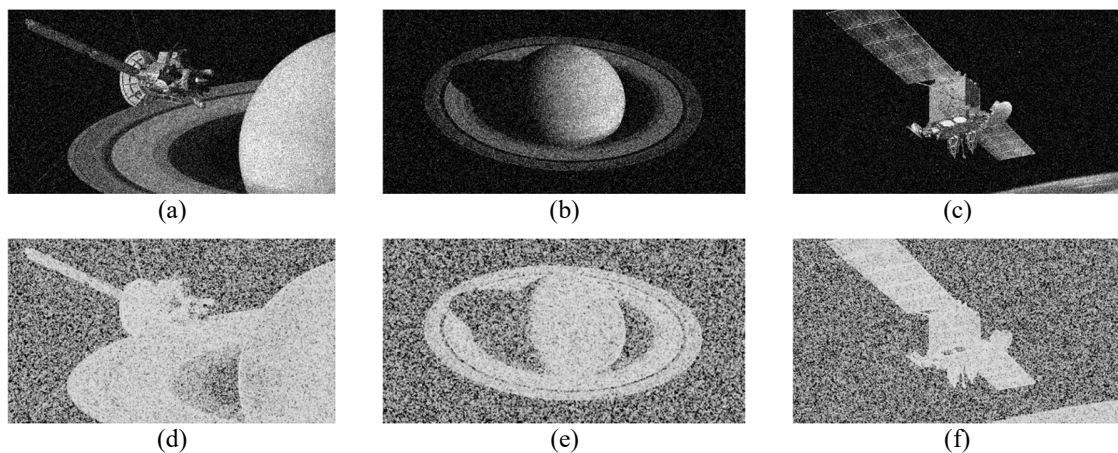

Figure 7. Noisy images and DS Transform results. **(a-c)** Noisy images (σ^2=40), **(d-f)** Results of Dissimilarity Transform.
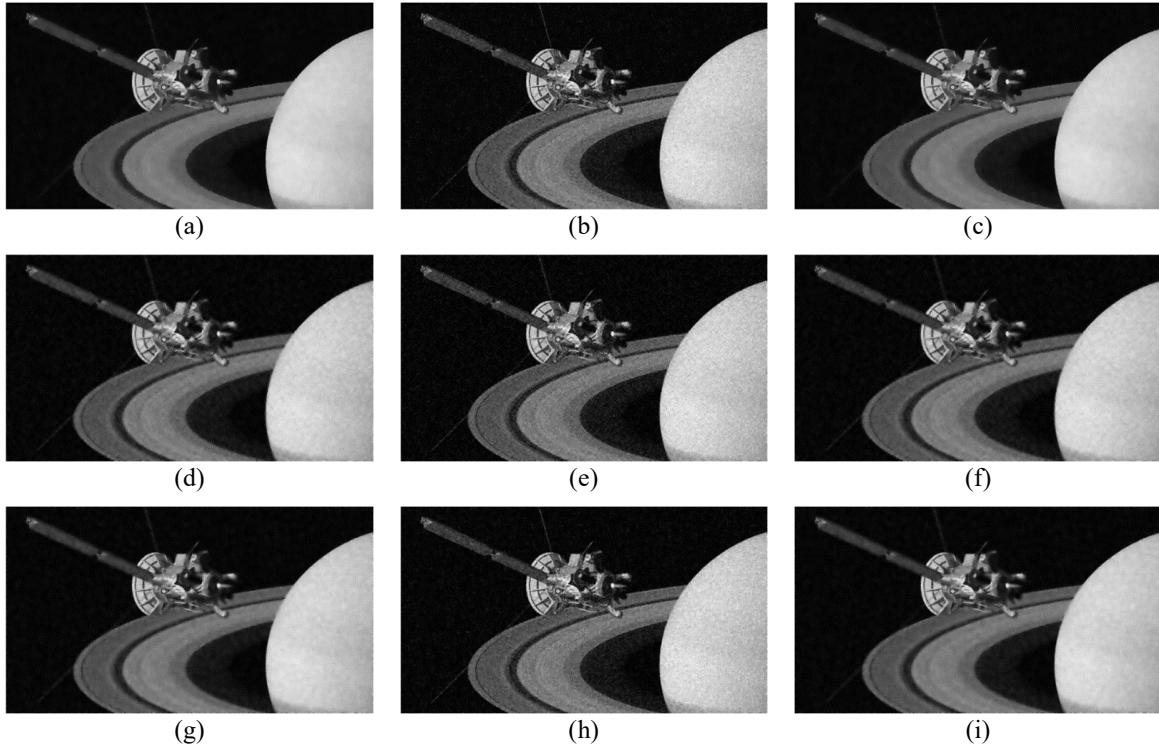
Figure 8. ADF results of the first noisy images (σ^2=20), **(a)** PM with K=10, **(b)** PM with TD, **(c)** PM with proposed model **(d)** YK with K=10, **(e)** YK with TD, **(f)** YK with proposed model, **(g)** PM with K=10, **(h)** PM with TD, **(i)** PM with proposed model.
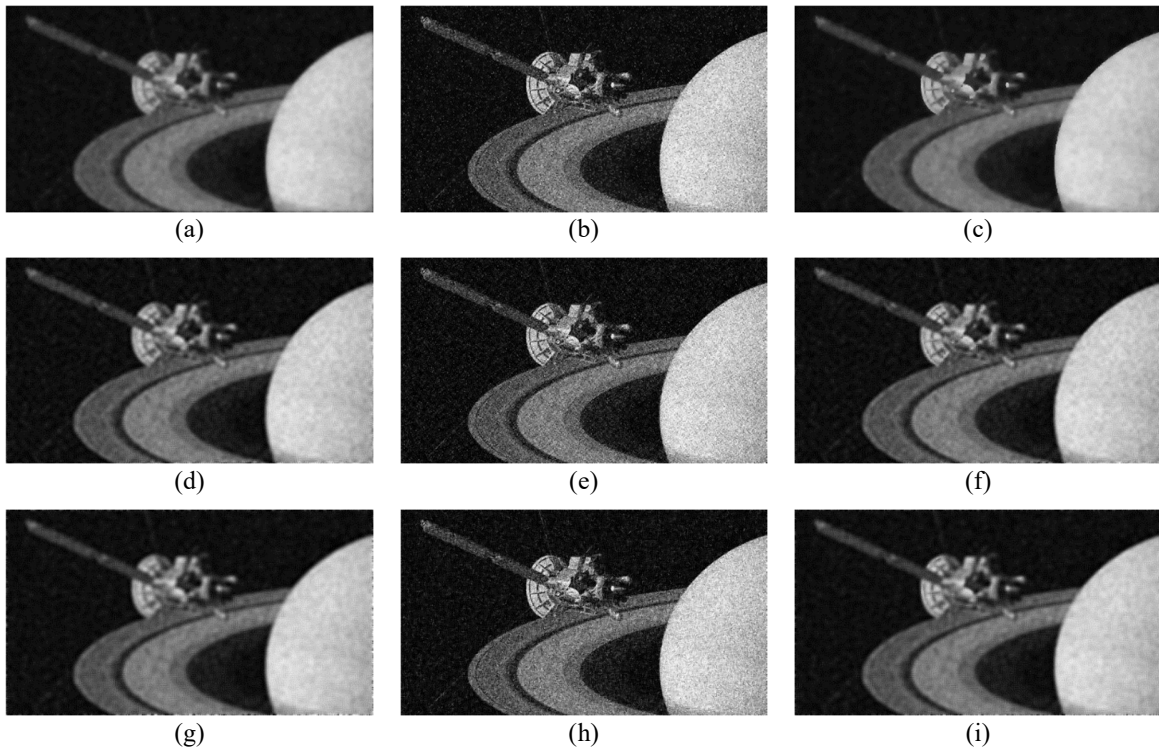

Figure 9. ADF results of the first noisy images (σ^2=40), **(a)** PM with K=75, **(b)** PM with TD, **(c)** PM with proposed model **(d)** YK with K=75, **(e)** YK with TD, **(f)** YK with proposed model, **(g)** PM with K=75, **(h)** PM with TD, **(i)** PM with proposed model.

The results of denosing for the first astronomical image with σ2 = 20 and σ2 = 40 gauss noise in Fig. 6(a) and Fig. 7(a) are given in Figs. 8 and 9. The rows contain the PM, YK, and HS results, respectively. The first column contains the results where the threshold value is constant and K = 10 for Fig. 8 and K = 75 for Fig. 9. In the second column, the K value is calculated with the TD approach, while in the third column it is calculated with the proposed method. In addition, the results of SSIM and PNSR obtained with PM,

YK, and HS at all noise levels of the image in Fig. 2(a) are included in Fig. 10. Both visual evaluations and results of SSIM and PSNR show that the PM approach has yielded very successful results. Also, in the graphs of the three denoising techniques, it is seen that the results obtained with the proposed threshold value approach are quite successful. The most successful results at all noise levels for PM, YK, and HS ADF techniques are obtained using the K threshold value determined by the proposed approach. Although the threshold values determined with the TD approach or selected as constant produce similar results with the proposed approach at various noise levels, they are negatively affected by the noise level change.

The visual evaluation of denoising success has been made with a perspective that has not been included in previous studies. The edge images for Figs. 8 and 9 detected by the LoG technique are shown in Figs. 11 and 12, respectively. The LoG technique is highly affected by noise when detecting edges and makes it very easy to identify noisy areas [26]. According to the results in Figs. 11 and 12, the success of the results using the proposed method is quite satisfactory in both high and low noise variances.

For the second astronomical noisy image with $\sigma^2 = 20$ and $\sigma^2 = 40$, denoising results are shown in Figs. 13 and 14. According to the SSIM and PSNR results in Fig. 15, it can be found that threshold values calculated with the proposed method get better denoising performance than the values of selected constant or calculated with the TD approach. Edge detection results using LoG technique in Figs. 16 and 17 show the proposed method more successfully than TD method. Moreover, the proposed method produces similar results with optimally selected constant values. It can be said that the proposed model in terms of noise reduction in visual evaluations is quite successful. The denoising results of the third noisy astronomical image ($\sigma^2 = 20$ and $\sigma^2 = 40$) are included in Figs. 18 and 19. Although SSIM results in Fig. 20(a-c) are quite similar for K values calculated by the proposed and TD methods, PSNR results in Fig. 20(d-f) show that the proposed approach is more successful. In addition, with the help of both SSIM and PSNR graphics, it is seen that the proposed approach is successful in all noise variances. The images in Figs. 21 and 22, which are used to make the visual assessment more specific, show that the proposed method has better noise removal and edge protection performance than the TD approach. In addition, the results of the proposed method are quite similar to those obtained with constant K values, as in the first two astronomical images. Examination of the experimental results shows the superiority of the proposed method. However, it is known that more effective results are obtained with neural network studies, which have become popular in recent years (Türk et al., 2020; Türk et al., 2019). In future studies, the proposed method should be integrated with neural network models to achieve more successful results and work with medical images.
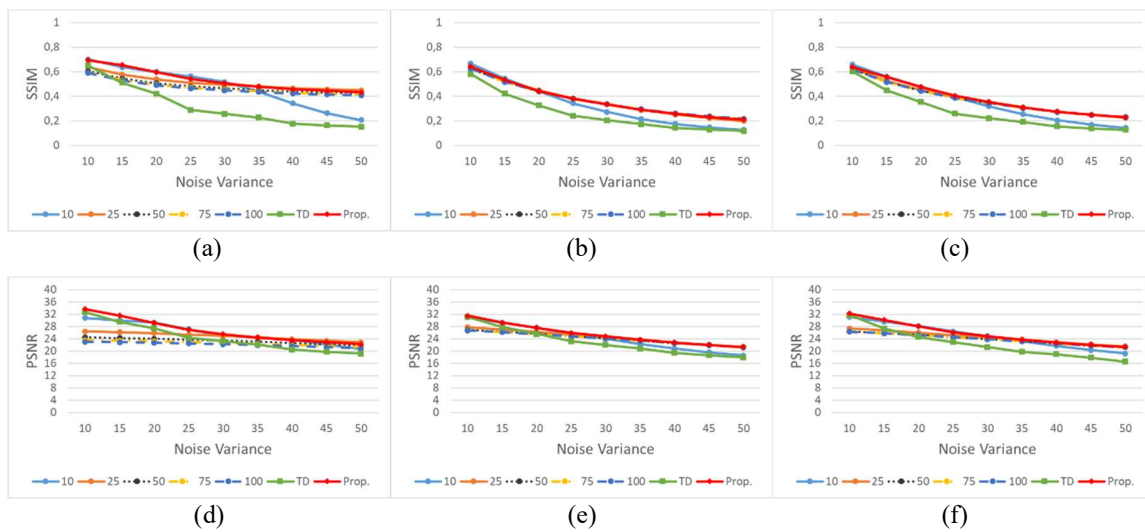

Figure 10. PSNR and SSIM results for denosing of the first noisy images. **(a)** SSIM results of PM. **(b)** SSIM results of YK. **(c)** SSIM results of HM. **(d)** PSNR results of PM. **(e)** PSNR results of YK. **(f)** PSNR results of HM.
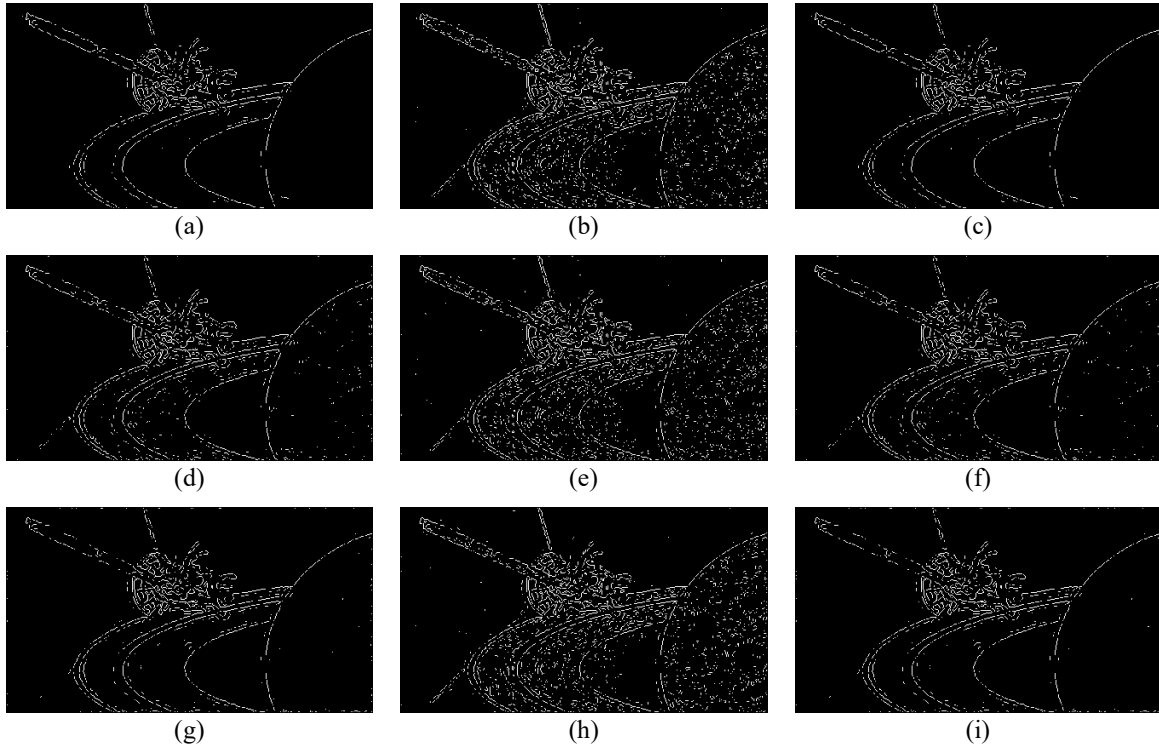
Figure 11. LoG Edge Detection results of denoised images in Fig. 8 (σ^2=20). **(a)** PM with K=10, **(b)** PM with TD, **(c)** PM with proposed model **(d)** YK with K=10, **(e)** YK with TD, **(f)** YK with proposed model, **(g)** PM with K=10, **(h)** PM with TD, **(i)** PM with proposed model.
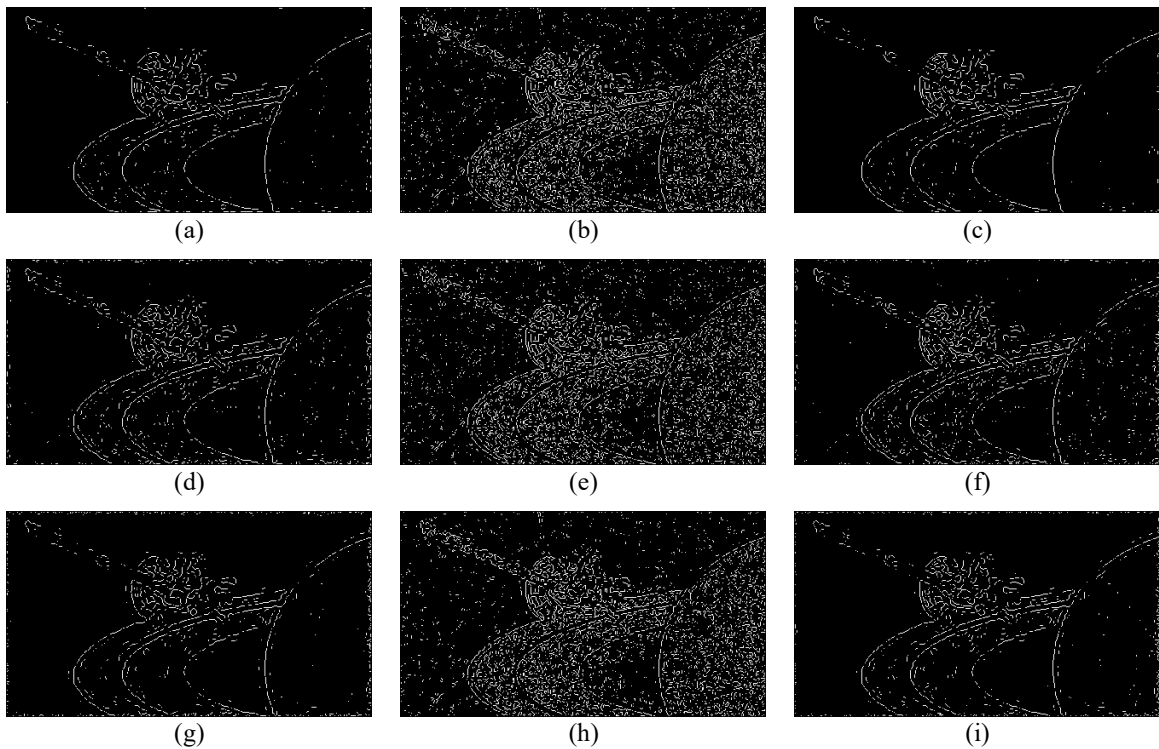

Figure 12. LoG Edge Detection results of denoised images in Fig. 9 (σ^2=40). **(a)** PM with K=75, **(b)** PM with TD, **(c)** PM with proposed model **(d)** YK with K=75, **(e)** YK with TD, **(f)** YK with proposed model, **(g)** PM with K=75, **(h)** PM with TD, **(i)** PM with proposed model.
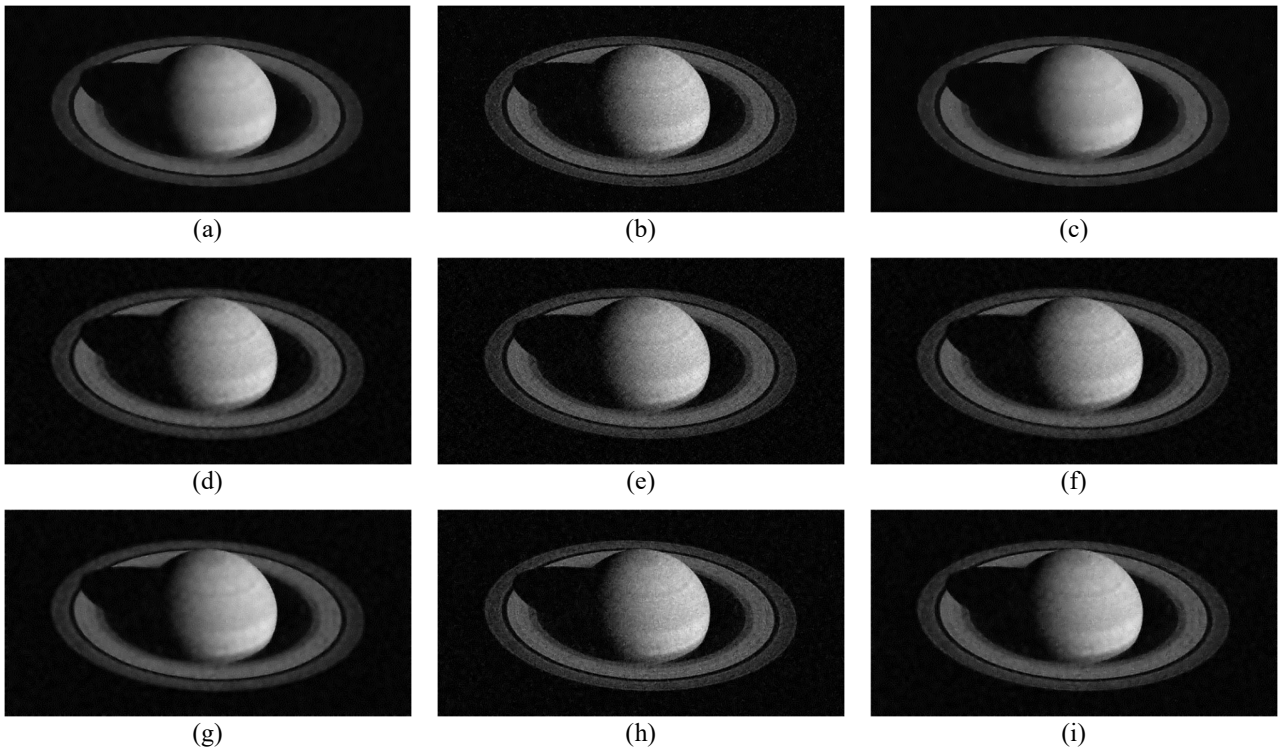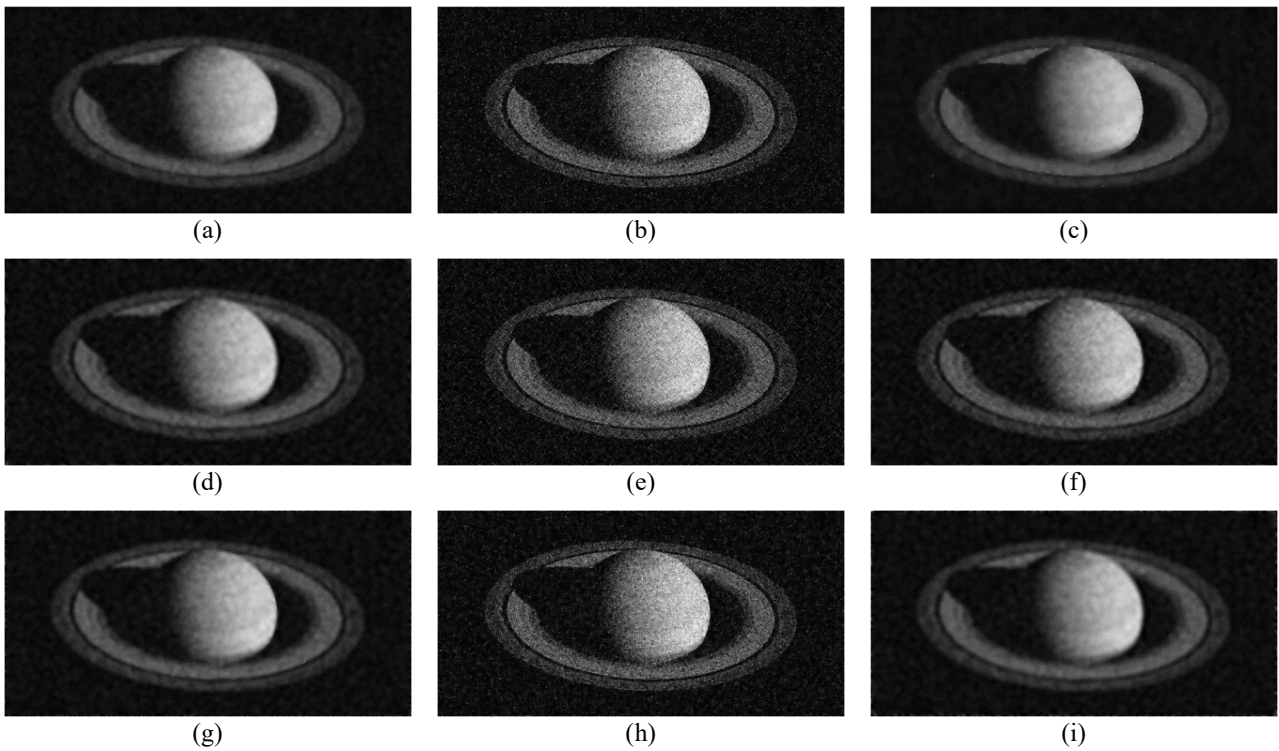
Figure 13. ADF results of the second noisy images ($\sigma^2=20$), **(a)** PM with K=10, **(b)** PM with TD, **(c)** PM with proposed model **(d)** YK with K=10, **(e)** YK with TD, **(f)** YK with proposed model, **(g)** PM with K=10, **(h)** PM with TD, **(i)** PM with proposed model.

Figure 14. ADF results of the second noisy images ($\sigma^2=40$), **(a)** PM with K=75, **(b)** PM with TD, **(c)** PM with proposed model **(d)** YK with K=75, **(e)** YK with TD, **(f)** YK with proposed model, **(g)** PM with K=75, **(h)** PM with TD, **(i)** PM with proposed model.
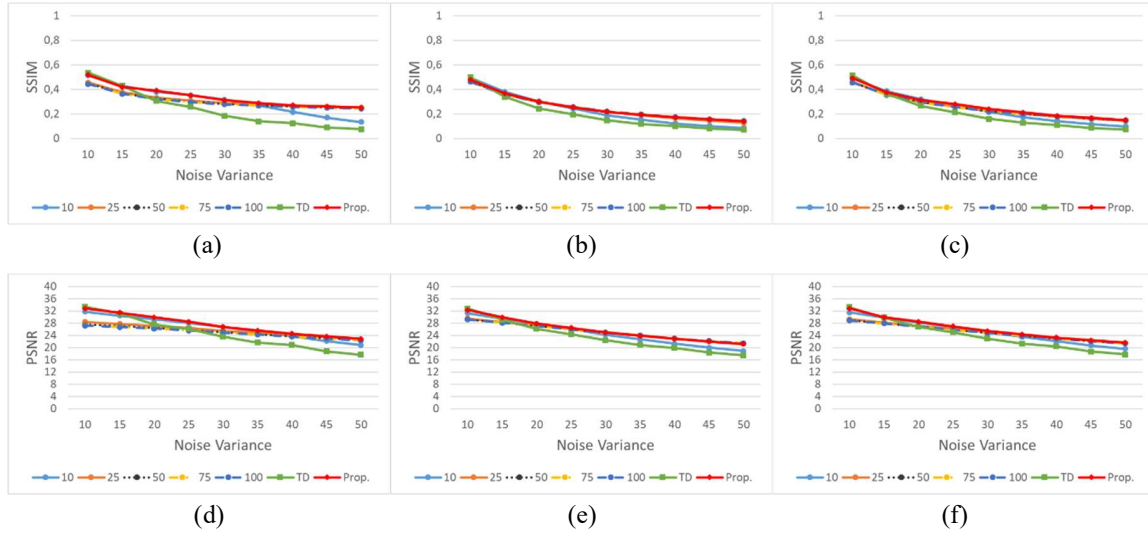
Figure 15. PSNR and SSIM results for denosing of the second noisy images. **(a)** SSIM results of PM. **(b)** SSIM results of YK. **(c)** SSIM results of HM. **(d)** PSNR results of PM. **(e)** PSNR results of YK. **(f)** PSNR results of HM.
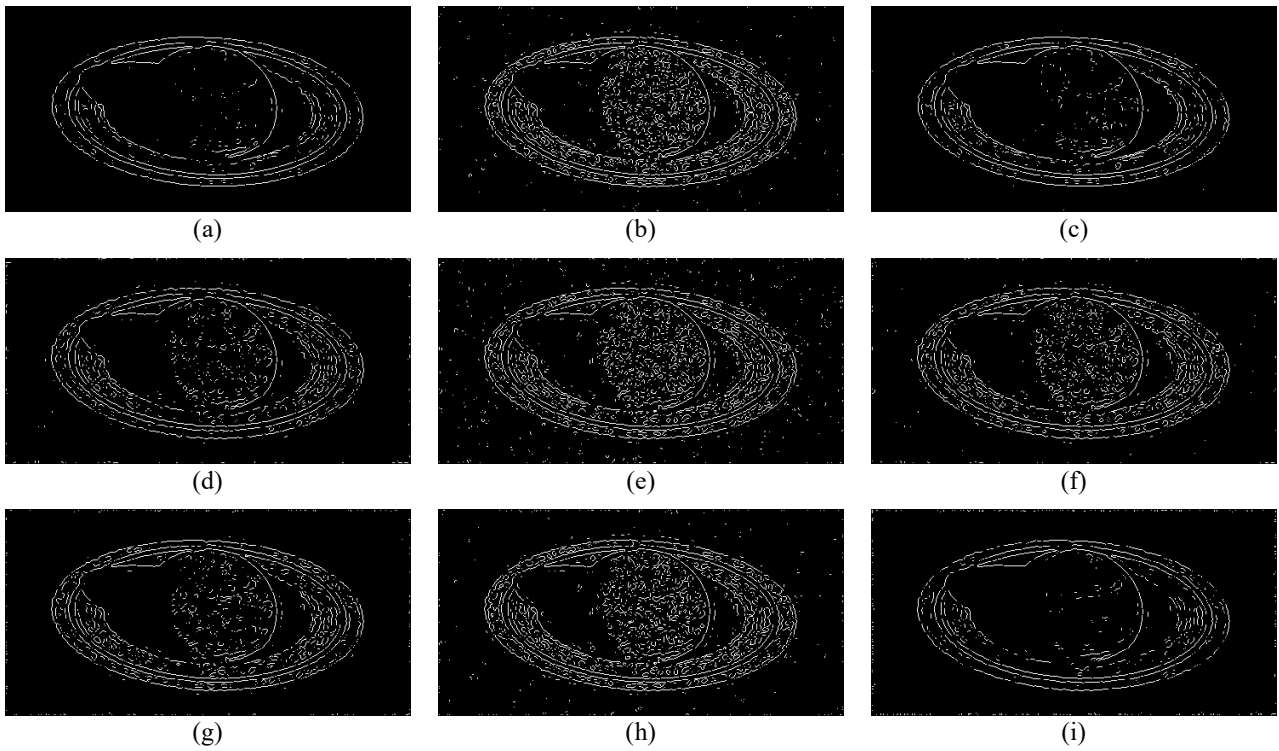

Figure 16. LoG Edge Detection results of denoised images in Fig. 13 ($\sigma^2=20$). **(a)** PM with K=10, **(b)** PM with TD, **(c)** PM with proposed model **(d)** YK with K=10, **(e)** YK with TD, (f) YK with proposed model, **(g)** PM with K=10, **(h)** PM with TD, (i) PM with proposed model.
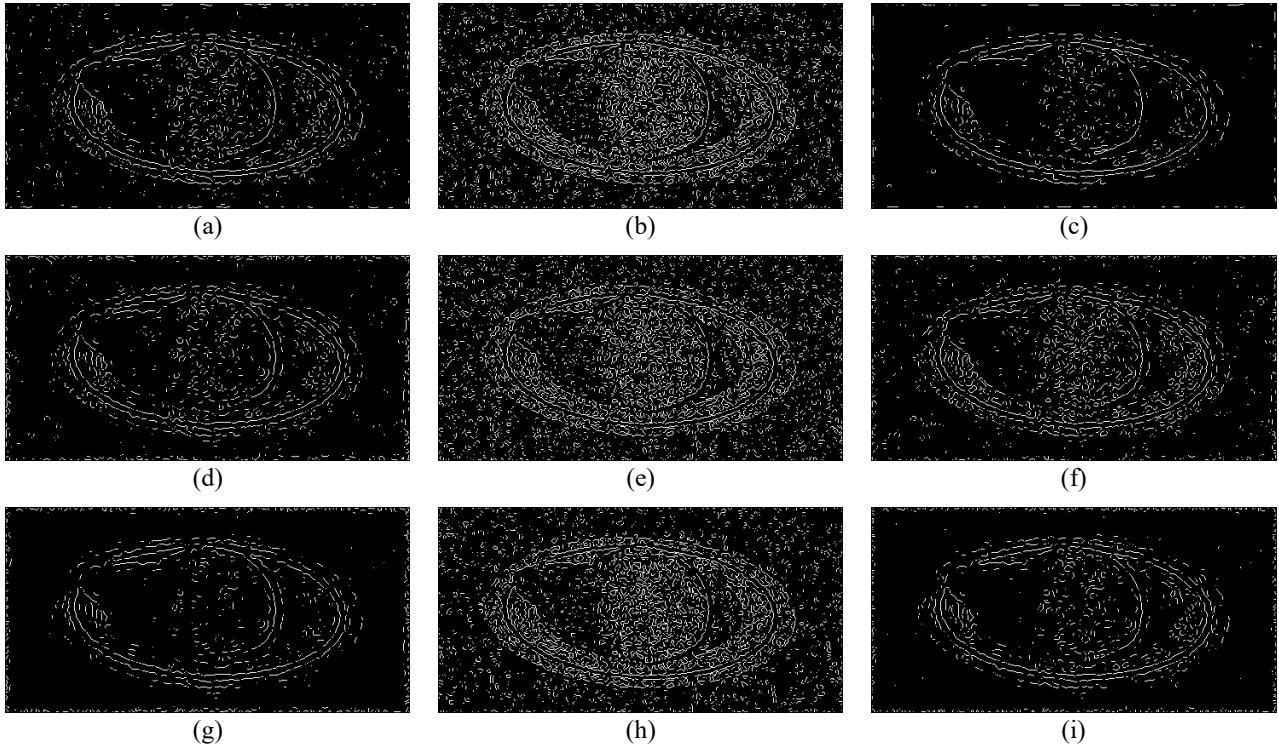
Figure 17. LoG Edge Detection results of denoised images in Fig. 14 (σ²=40). **(a)** PM with K=75, **(b)** PM with TD, **(c)** PM with proposed model **(d)** YK with K=75, **(e)** YK with TD, **(f)** YK with proposed model, **(g)** PM with K=75, **(h)** PM with TD, (i) PM with proposed model.

Figure 18. ADF results of the third noisy images (σ²=20), **(a)** PM with K=10, **(b)** PM with TD, **(c)** PM with proposed model **(d)** YK with K=10, **(e)** YK with TD, **(f)** YK with proposed model, **(g)** PM with K=10, **(h)** PM with TD, **(i)** PM with proposed model.
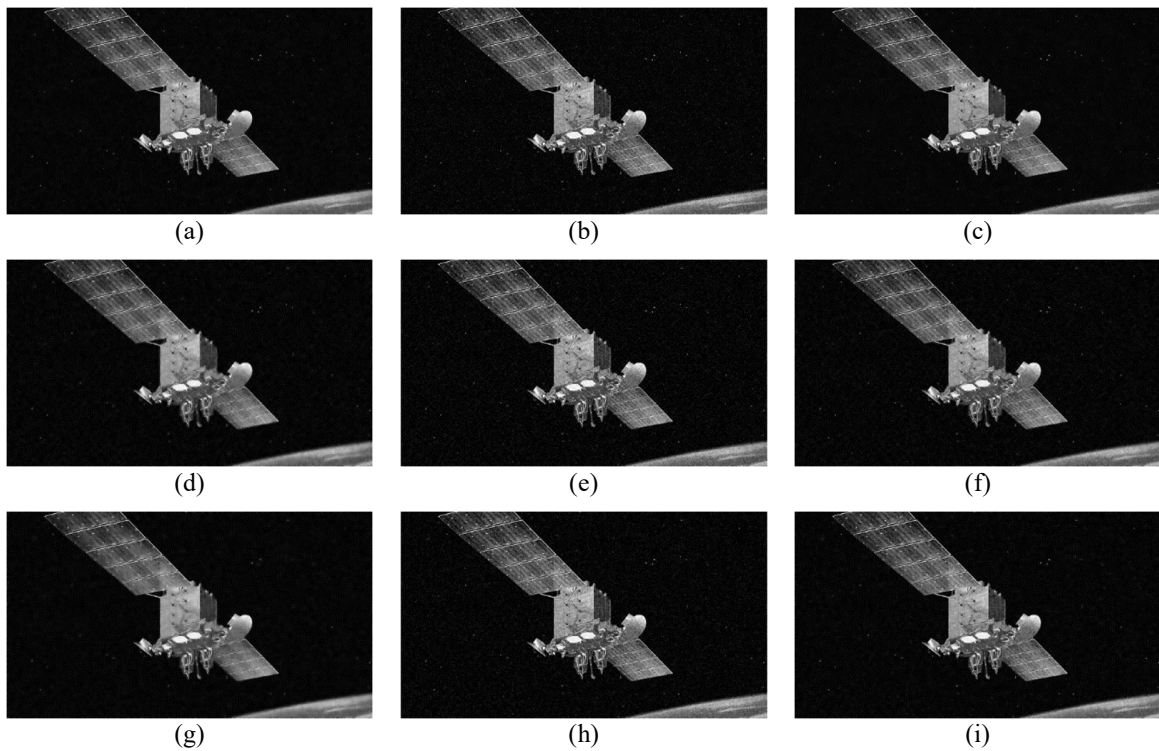
Figure 19. ADF results of the third noisy images (σ²=40), **(a)** PM with K=75, **(b)** PM with TD, **(c)** PM with proposed model **(d)** YK with K=75, **(e)** YK with TD, **(f)** YK with proposed model, **(g)** PM with K=75, **(h)** PM with TD, **(i)** PM with proposed model.
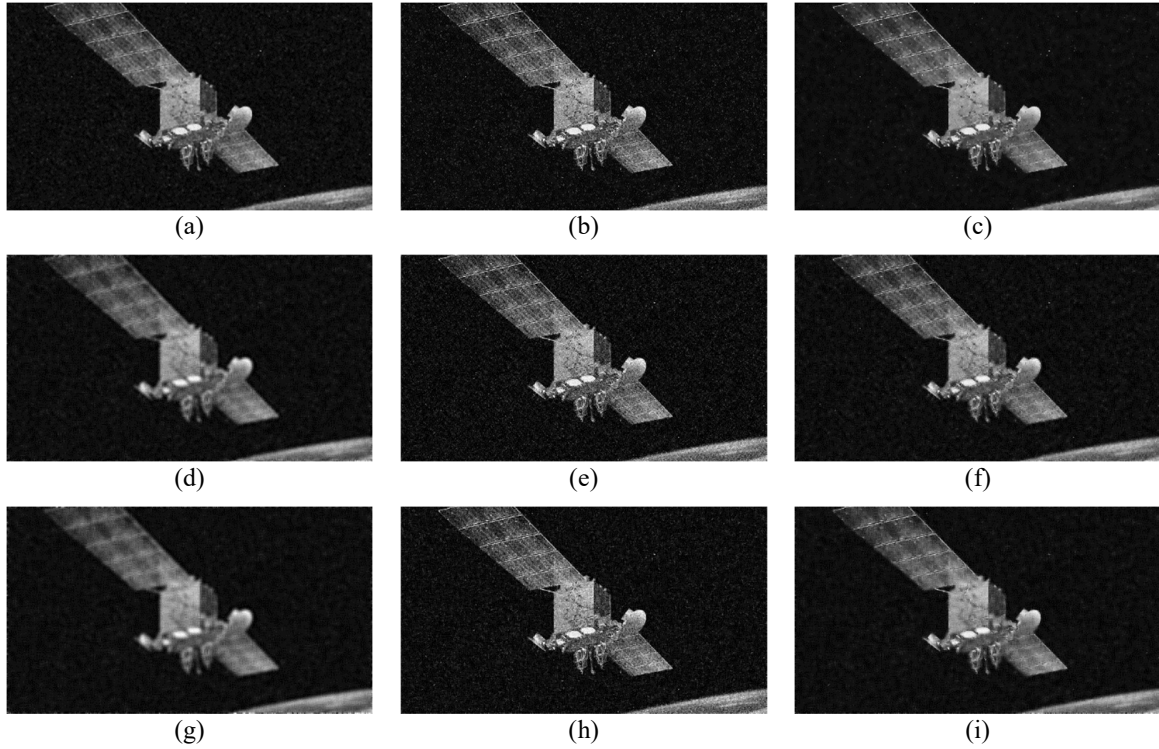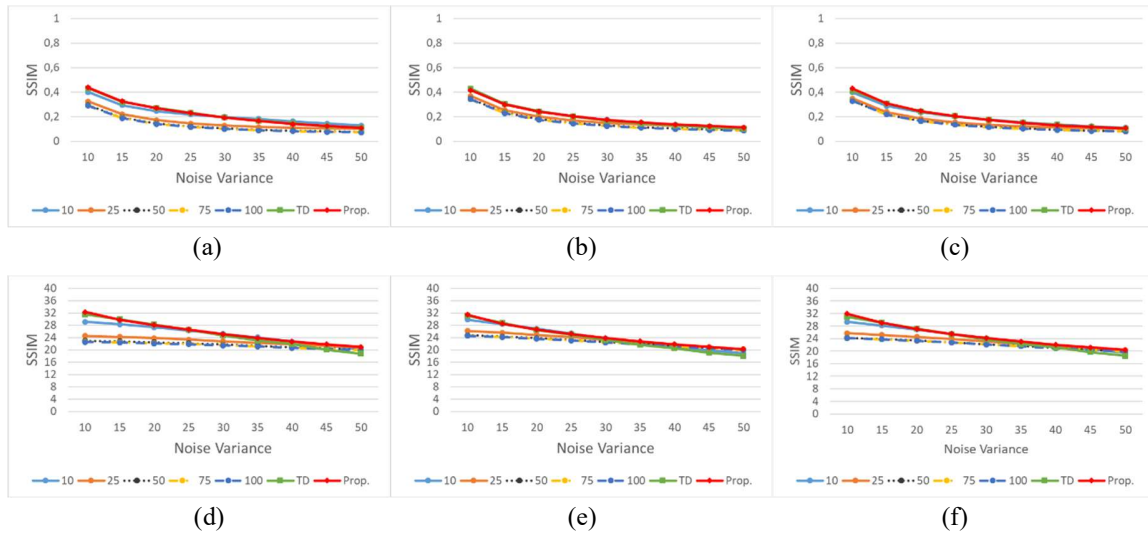

Figure 20. PSNR and SSIM results for denosing of the third noisy images. **(a)** SSIM results of PM. **(b)** SSIM results of YK. **(c)** SSIM results of HM. **(d)** PSNR results of PM. **(e)** PSNR results of YK. **(f)** PSNR results of HM.

Figure 21. LoG Edge Detection results of denoised images in Fig. 18 (σ^2=20). **(a)** PM with K=10, **(b)** PM with TD, **(c)** PM with proposed model **(d)** YK with K=10, **(e)** YK with TD, **(f)** YK with proposed model, **(g)** PM with K=10, **(h)** PM with TD, **(i)** PM with proposed model.
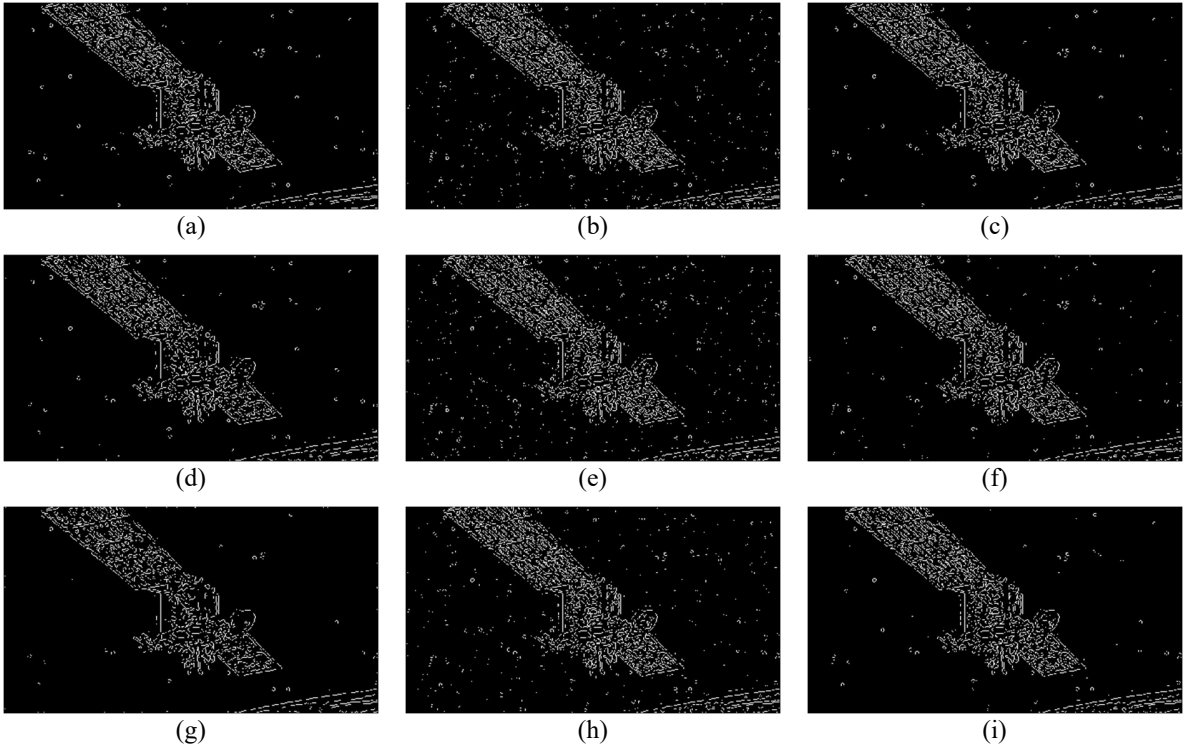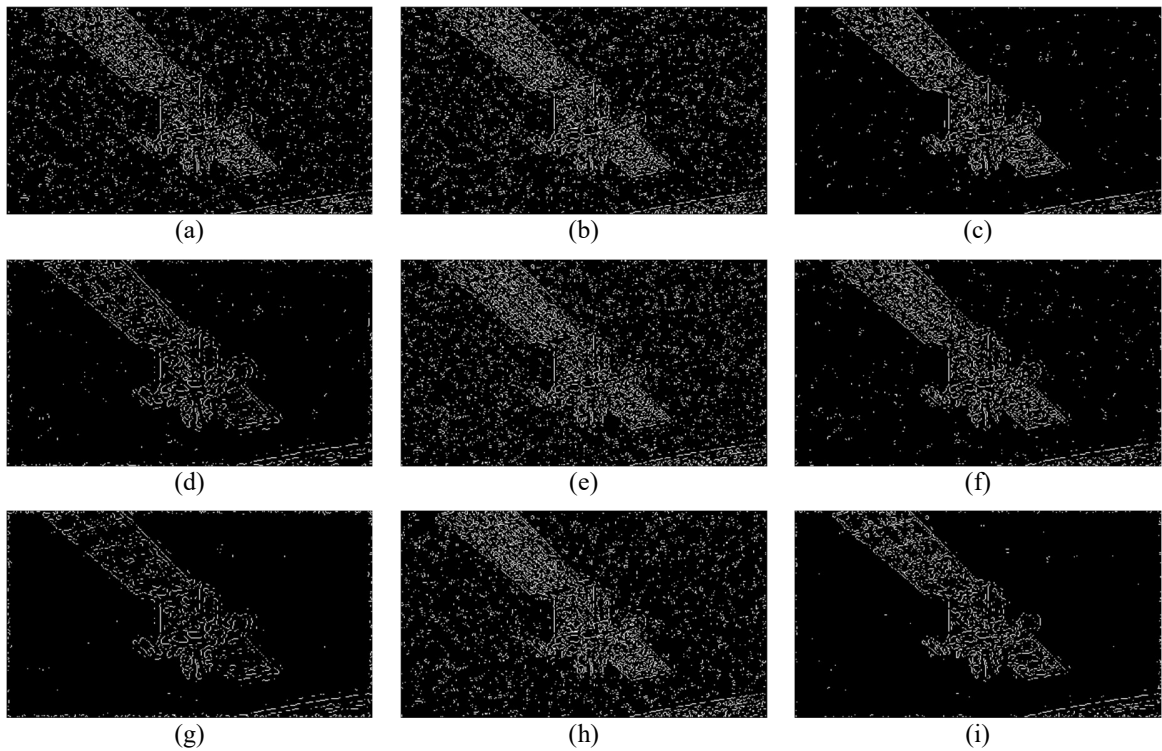

Figure 22. LoG Edge Detection results of denoised images in Fig. 19 (σ^2=40). **(a)** PM with K=75, **(b)** PM with TD, **(c)** PM with proposed model **(d)** YK with K=75, **(e)** YK with TD, **(f)** YK with proposed model, **(g)** PM with K=75, **(h)** PM with TD, **(i)** PM with proposed model.

4. Conclusion

In this study, a new adaptive method based on dissimilarity of pixels is proposed to determine the diffusion threshold value of anisotropic diffusion filters. In the proposed model, pixel dissimilarity is introduced to general ADFs. With the help of this model, it is no longer necessary for the user to determine a threshold value or to select different threshold values by trial and error. The proposed approach is tested using both conventional and fourth order ADFs. According to the experimental results, the threshold values determined adaptively with the help of the proposed method have the most successful denoising performance in all noise variances, while also protecting the edges. It is planned that the proposed approach in future studies will be applied on medical images by increasing the effectiveness of neural network structures.

Referanslar

Aja-Fernández, S., & Alberola-López, C. (2006). On the estimation of the coefficient of variation for anisotropic diffusion speckle filtering. *IEEE Transactions on Image Processing*, *15*(9), 2694-2701.

Ali, H. (2013). Fast Color Edge Detection Algorithm Based on Similarity Relation Matrix. *International Journal of Computer Science Issues (IJCSI)*, *10*(5), 108.

Aydın, M., Hardalaç, F., Ural, B., & Karap, S. (2016). Neonatal jaundice detection system. *Journal of medical systems*, *40*, 1-11.

Barbu, T. (2016). A hybrid nonlinear fourth-order PDE-based image restoration approach. 2016 20th International Conference on System Theory, Control and Computing (ICSTCC),

Charbonnier, P., Blanc-Feraud, L., Aubert, G., & Barlaud, M. (1994). Two deterministic half-quadratic regularization algorithms for computed imaging. Proceedings of 1st international conference on image processing,

Demirci, R. (2007). Similarity relation matrix-based color edge detection. *AEU-international Journal of Electronics and Communications*, *61*(7), 469-477.

Demirci, R., Guvenc, U., & Tanyeri, U. (2012). Anisotropic diffusion filter without conductivity parameters. 2012 16th International Conference on System Theory, Control and Computing (ICSTCC),

Demirci, R., & Tanyeri, U. (2012). Anisotropic diffusion filter using Haar wavelet. 2012 16th International Conference on System Theory, Control and Computing (ICSTCC),

Deng, L., Zhu, H., Yang, Z., & Li, Y. (2019). Hessian matrix-based fourth-order anisotropic diffusion filter for image denoising. *Optics & Laser Technology*, *110*, 184-190.

Gao, L., Yao, D., Li, Q., Zhuang, L., Zhang, B., & Bioucas-Dias, J. M. (2017). A new low-rank representation based hyperspectral image denoising method for mineral mapping. *Remote sensing*, *9*(11), 1145.

Guvenc, U., Elmas, C., & Demirci, R. (2008). Automatic Segmentation of Color Images. *JOURNAL OF POLYTECHNIC-POLITEKNIK DERGISI*, *11*(1), 9-12.

Hajiaboli, M. R. (2009). A self-governing hybrid model for noise removal. Advances in Image and Video Technology: Third Pacific Rim Symposium, PSIVT 2009, Tokyo, Japan, January 13-16, 2009. Proceedings 3,

Ham, B., Min, D., & Sohn, K. (2012). Robust scale-space filter using second-order partial differential equations. *IEEE Transactions on Image Processing*, *21*(9), 3937-3951.

Incelas, M. O., Demirci, R., Yavuzcan, H. G., Tanyeri, U., & Veske, E. (2014). Seeded region growing based detection of cells in fish blood stained with Natt-Herrick. 2014 22nd Signal Processing and Communications Applications Conference (SIU),

Incetas, M. O., Demirci, R., & Yavuzcan, H. G. (2014). Automatic segmentation of color images with transitive closure. *AEU-international Journal of Electronics and Communications*, *68*(3), 260-269.

INCETAS, M. O., Demirci, R., & YAVUZCAN, H. G. (2019). Automatic color edge detection with similarity transformation. *Gazi University Journal of Science*, *32*(2), 458-469.

İncetaş, Tanyeri, U., Kılıçaslan, M., Yakışır Girgin, B., & Demirci, R. (2017). Eşik Seçiminin Benzerliğe Dayalı Kenar Belirlemeye Etkisi. 1st International Symposium on Multidisciplinary Studies and Innovative Technologies, Tokat/Turkey.

İncetaş, M. O., & Uçar, M. (2021, 16-18 May). *İğnecikli sinir ağina dayali benzerlik dönüşümü* ISPEC 10th INTERNATIONAL CONFERENCE ON ENGINEERING & NATURAL SCIENCES, Siirt/Turkey.

İncetaş, M. O., VESKE, E., Nesrin, E., & DEMİRCİ, R. (2017). Automatic cells counting in Natt-Herrick stained fish blood. *Aquaculture Studies*, *17*(3), 283-294.

Jain, P., & Tyagi, V. (2016). A survey of edge-preserving image denoising methods. *Information Systems Frontiers*, *18*, 159-170.

Perona, P., & Malik, J. (1990). Scale-space and edge detection using anisotropic diffusion. *IEEE Transactions on pattern analysis and machine intelligence*, *12*(7), 629-639.

Rafsanjani, H. K., Sedaaghi, M. H., & Saryazdi, S. (2016). Efficient diffusion coefficient for image denoising. *Computers & Mathematics with Applications*, *72*(4), 893-903.

Rafsanjani, H. K., Sedaaghi, M. H., & Saryazdi, S. (2017). An adaptive diffusion coefficient selection for image denoising. *Digital Signal Processing*, *64*, 71-82.

Tanyeri, U., & Demirci, R. (2018). Wavelet-based adaptive anisotropic diffusion filter. *Advances in Electrical and Computer Engineering*, *18*(4), 99-106.

Tsiotsios, C., & Petrou, M. (2013). On the choice of the parameters for anisotropic diffusion in image processing. *Pattern Recognition*, *46*(5), 1369-1381.

Türk, F., Lüy, M., & Barışçı, N. (2020). Kidney and renal tumor segmentation using a hybrid V-Net-based model. *Mathematics*, *8*(10), 1772.

Türk, F., Murat, L., & BARIŞÇI, N. (2019). Machine learning of kidney tumors and diagnosis and classification by deep learning methods. *International Journal of Engineering Research and Development*, *11*(3), 802-812.

Wang, Z., Bovik, A. C., Sheikh, H. R., & Simoncelli, E. P. (2004). Image quality assessment: from error visibility to structural similarity. *IEEE Transactions on Image Processing*, *13*(4), 600-612.

Weickert, J. (1998). *Anisotropic diffusion in image processing* (Vol. 1). Teubner Stuttgart.

Xu, J., Jia, Y., Shi, Z., & Pang, K. (2016). An improved anisotropic diffusion filter with semi-adaptive threshold for edge preservation. *Signal Processing*, *119*, 80-91.

You, Y.-L., & Kaveh, M. (2000). Fourth-order partial differential equations for noise removal. *IEEE Transactions on Image Processing*, *9*(10), 1723-1730.

Yu, J., Tan, J., & Wang, Y. (2010). Ultrasound speckle reduction by a SUSAN-controlled anisotropic diffusion method. *Pattern Recognition*, *43*(9), 3083-3092.